ICAS 2020 SHANGHAI
International Council of the Aeronautical Sciences
32nd Congress of the International Council of the Aeronautical Sciences
September 6-10, 2021
Pudong Shangri-La, Shanghai, China

NUMERICAL INVESTIGATION OF WING ROCK PHENOMENON ON LOW ASPECT RATIO RECTANGULAR WINGS AT LOW REYNOLDS NUMBER

Aamir Sultan[1], Adnan Maqsood[1], Tiauw Hiong Go[2] & Rizwan Riaz[1]

[1]National University of Sciences & Technology, Islamabad, Pakistan 44000
2 Raytheon Missile Systems, Tucson, Arizona

Abstract

Wing rock is a highly nonlinear undesirable phenomenon involving lateral directional instabilities at higher angles of attack and subsonic speeds. This study investigates the wing rock phenomenon on a rectangular wing of aspect ratio two and Reynolds number of 100,000. These conditions are typical of fixed-wing Micro Air Vehicles (MAV). The experimental study, conducted in a low-speed wind tunnel, successfully captures wing rock through free-to-roll experiments. In the vicinity of the stall, the onset of wing-rock was observed. To further the investigation, a numerical study is conducted to find the static and dynamic stability derivatives in a roll from 0˚ to 30˚ angle of attack and a reduced frequency of 0.0346 through forced roll oscillations of 40˚ amplitude. The conditions of wind-tunnel tests are replicated in numerical simulations. The forced roll oscillations on the rectangular wing were implemented through the sliding mesh technique in a commercial CFD solver. The loss in roll moment damping, a sufficient condition of wing rock, was observed in the vicinity of the stall. The flow physics of the vortex dynamics revealed that the wing rock phenomenon starts to occur due to the bursting of the side tip vortex and its interaction with the leading edge separated vortex around the stall.

Keywords: wing rock, roll oscillation, roll damping, vortex breakdown

1. Introduction

Wing rock is a Limit Cycle Oscillation (LCO) phenomenon in which an aircraft undergoes roll oscillation about its longitudinal axis. It tends to fly at higher angles of attacks while cruising at subsonic speeds. The wing rock oscillations involve multiple degrees of freedom, but due to the complexity of motion, it is mainly studied considering only one degree of freedom. The sustainment of the wing rock phenomenon could drastically affect the stability, control, and maneuverability characteristics of an aircraft. The presence of roll oscillations has adverse effects on the handling capabilities of a pilot sitting in the cockpit. Thus, it could lead to some catastrophic outcomes if not alleviated within a specific time frame. A great deal of work has been done in the past to decipher the dynamics and resulting flow physics of the wing rock phenomenon.

Initially, fighter aircraft with highly swept and delta wings were reported to experience this highly nonlinear wing rock limit cycle oscillation phenomenon [1]. The coupled effects of possession of little roll damping and the highly time-dependent nature of the leading-edge vortices made these wing configurations susceptible to these self-sustained roll oscillations. At the onset of the wing rock phenomenon, the amplitude of roll oscillations starts to increase initially. However, ultimately reaching a constant amplitude gives rise to the phenomenon of limit cycle oscillation [2]. The oscillatory characteristics of the wing rock phenomenon are linked with the nonlinear nature of the rolling moment coefficient. There are two flight regimes at which wing rock is experienced; at low subsonic speed while flying at higher angles of attack and in transonic regime at moderate angles of attack [3].

The causation of the latter is attributed to the shock resulting in stall/un-stall phenomenon. Ericsson [4, 5] deciphered the slender wing rock phenomenon on delta wings, suggesting that asymmetry in leading-edge vortices gives rise to these roll oscillations. Moreover, it was postulated that delta wings with moderate sweep angles are also prone to the wing rock phenomenon, proposing the asymmetry in fore-body vortices as the causation of these oscillations on such wing configurations.

The asymmetry in leading-edge vortices could arise due to asymmetric behavior in their position, strength, or breakdown phenomenon [6]. Several research studies [1,7,8] have been reported in the literature on the dynamics of vortical structures found on delta wings whose asymmetric behavior is thought to be the reason for the onset of the wing rock phenomenon. Ross [9] suggested that the wing rock phenomenon's initiation on slender wings depends on the inherent design characteristics of these wing configurations. He attributed the onset of wing rock phenomenon on slender wings to the lack of roll damping at higher angles of attack. Further, he added that decreasing the angle of attack or activating the roll control surfaces could effectively alleviate these oscillations. Jun and Nelson [7], in their experimental studies on delta wings, extracted the vortex core positions of leading-edge vortices during the wing rock cycle and discovered that even at a roll angle of 0 deg, the vortex core positions of the left and right vortex are at different vertical heights. This spatial difference in vortex core positions acts as an initial perturbation to initiate wing rock. Nguyen *et al.* [10] studied the effects of the sideslip angle on the roll damping parameter. They found that increasing the sideslip angle results in an enhanced roll damping capability of the system hence preventing the onset of the wing rock phenomenon.

Wing rock on delta wings was present because of an inherent asymmetry in leading-edge vortices. However, very little work has been done to decipher the wing rock on rectangular wings planform. The study of wing rock on rectangular wing planform is essential because these planforms are pretty commonly used in Micro Air Vehicles (MAVs) [11-12] and small Unmanned Air Vehicles (sUAVs) [13-14]. MAV must have good maneuverability and a prolonged endurance limit to maintain a slow and forward-speed flight [15-16]. Rectangular wings have two side-tip vortices. The interaction of these vortices with the leading-edge vortex can give rise to instabilities at such higher angles of attack.

Low aspect ratio rectangular wings possess some unique and peculiar aerodynamic characteristics. In addition to the linear lift, which is generated due to the circulation of flow around the wing, they also generate nonlinear lift, mainly due to additional wingtip vortices. Separation bubbles and laminar to turbulent transition make this flow regime even more complex to study. Studying the distribution of lift across wings is essential to decipher the wing rock phenomenon on low aspect ratio rectangular wings. The flow peculiarities and distinct vortices structure on low aspect ratio rectangular wing at low Reynolds number make it different from conventional wing rock phenomenon on delta wings.

In this paper, the phenomenon of wing rock is deciphered on a rectangular wing of aspect ratio 2. Initially, the free-to-roll experiment is performed in a low subsonic wind tunnel, and the onset of wing rock in the vicinity of the stall is captured. Subsequently, to visualize the vortex dynamics and causation of wing rock, computational fluid dynamic simulations are performed for the same amplitude and frequency recorded during the experiments. The onset of wing rock, primarily attributed to loss of damping in roll, is linked with the flow physics of vortex burst phenomena.

2. Problem Formulation

2.1 Experimental Setup

The experiment is performed in a closed-circuit subsonic wind-tunnel with a maximum documented turbulence level of 0.1% in any direction. The dimensions of the rectangular test-section are 0.78x0.72 m. Aerodynamic loads and moments are measured through a six-component internal balance. A rectangular wing of aspect ratio 2, having a chord length of 0.2032 m, and thickness to chord ratio of 1.96 %, is used. The leading and trailing edges of the rectangular wing are 5-to-1 elliptical in shape. The geometry of the wing is taken from the literature [7, 17]. The experimental setup is depicted in Figure 1. For details, the readers are referred to the study performed by Go & Maqsood [18].

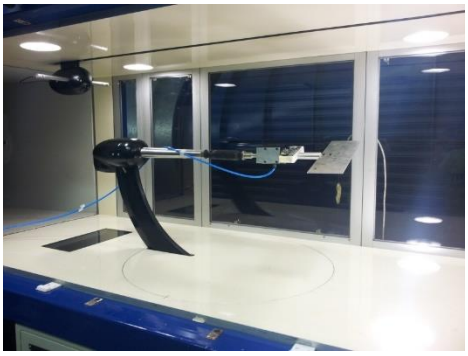

Figure 1– Experimental setup of free-to-rotate rectangular-wing (AR=2)

The free-to-roll tests are conducted at a constant freestream velocity of 12.6 m/s. Figure 2 shows the variation of roll amplitude with angles of attack. It can be observed that the rectangular wing does not display wing rock phenomena till the 16 deg angle of attack. The self-excited roll oscillations are observed only beyond that, and the amplitude increase with the increase in the angle of attack. The phase plot of roll oscillations is also plotted in Figure 2. In this instance, the amplitude of the oscillations was approximately 0.8 rad (46°), and the roll rate was about 5.0 rad/s (286°/s). The small asymmetrical features can be attributed to minor variation in the mass distribution of the model apparatus.

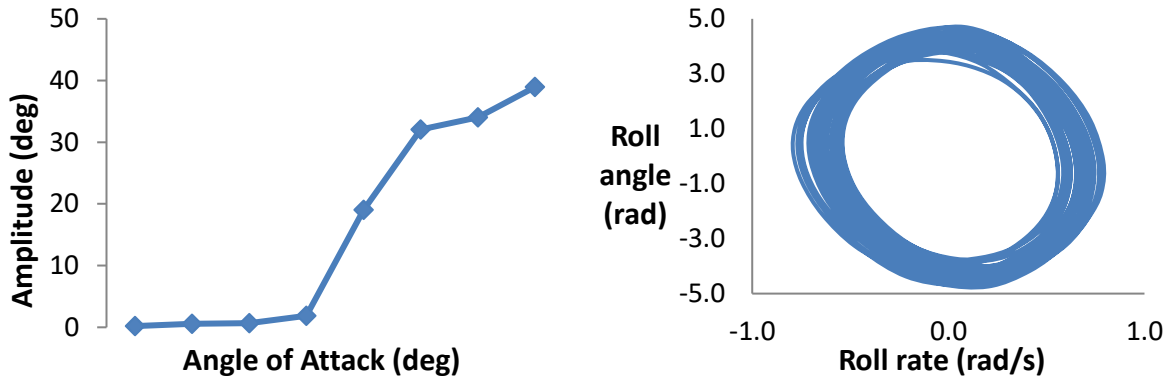

Figure 2– Variation of amplitude with the increase in angle of attack (left) and representative phase portrait (right)

2.2 Computational Modeling

High-quality grid generation is considered a fundamental and essential step in performing a computational fluid dynamic simulation. It greatly influences the accuracy of results and stability of the numerical simulation. The sliding mesh technique requires two domains, the inner rotating domain and an external static domain which are later merged, forming an interface zone. An unstructured tetra grid was generated on inner and outer domain of the 3D case. The schematic representation of the gird on the inner and outer zone of the 3D case is shown in Figure 3.

The boundary condition used in the computational setup is also labeled. A pressure far-field boundary condition was applied on the outermost circular boundary. A non-slip wall boundary condition was used, and an interface zone boundary condition was applied where the static and rotating zones were meeting together. Five meshes of different sizes were generated during the grid independence study and were compared based on lift and drag coefficients. At the end of the mesh independence study, the optimum mesh size was chosen. Three turbulence models, kω-SST, kϵ -Realizable, and SA models, were tested against the experimental results of lift and drag coefficients. It is noticed that the results of the SA model are in good agreement with the experimental results of lift and drag coefficients.

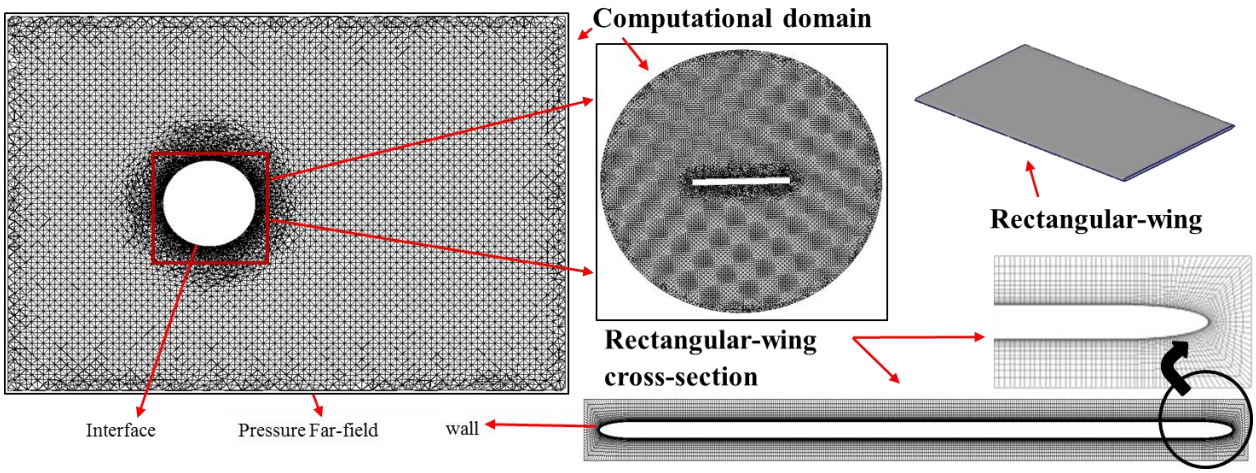

Figure 3 – Computational domain, sliding mesh interface, wing-cross-section, and near-surface mesh of rectangular wing with aspect ratio 2

SA model is a one equation turbulence model in which the transport equation is solved for the kinematic eddy turbulent viscosity. SA model in its original form is a low Reynolds number turbulence model. It is used for aerospace applications and can accurately solve boundary layers with adverse pressure gradients. The mathematical expression for the SA turbulence model is presented in the following equations

$$\mu\Delta\overline{u_\iota} - \rho\left(\frac{\partial\overline{u_\iota u_J}}{\partial x_j}\right) = \mu\frac{\partial}{\partial x_j}\left(\frac{\partial u_i}{\partial x_j}\right) - \rho\frac{\partial}{\partial x_j}\left(\overline{u_\iota u_J}\right) \quad (1)$$

The term $\left(\frac{\partial\overline{u_\iota u_J}}{\partial x_j}\right)$ is referred to as Reynolds-Stresses. The expression $\left(\mu\frac{\partial u_i}{\partial x_j} - \rho\left(\overline{u_\iota u_J}\right)\right)$ is termed total shear stress τ_{ij} . On incorporating the concept of the eddy viscosity model, the expression for total shear stress τ_{ij} becomes

$$\tau_{ij} = \mu\frac{\partial u_i}{\partial x_j} + \rho\left(V_T\left(\frac{\partial u_i}{\partial x_j} + \frac{\partial u_j}{\partial x_i}\right) - \frac{2}{3}k\delta_{ij}\right) \quad (2)$$

Oscillatory characteristics of the forced roll oscillations from the experimental data are shown in Table 1. The oscillatory characteristics of forced roll oscillation were applied on the rotatable inner fluid zone through a time-varying sine wave function. A user-defined function was compiled and fed into the static analysis case file through which dynamic simulations were run. A time independence study was conducted for running dynamic simulations. Initially, three-time step sizes were checked. The time step size of 0.005 s results started to diverge, so the time step was decreased to 0.001 and 0.0008, respectively. Both of the time step sizes of 0.001 and 0.0008 showed similar results. Hence the optimum time step size of 0.001 was chosen for running dynamic simulations. The schematic of the time independence study is shown in Figure 4. Dynamic simulations were run for three successive cycles of forced roll oscillations. The last two cycles of oscillations repeated similar results of the rolling moment coefficient. Hence the second cycle of oscillation was considered for further studies. The schematic of convergence criteria for dynamic simulations is also depicted in Figure 4.

Table 1– Attributes of forced oscillations

No.	Attribute (units)	Value
1	Oscillation Frequency (Hz)	1
2	Reduced Frequency	0.085
3	Amplitude (deg)	40
4	No. of time-steps per cycle	1000
5	No. of oscillation cycles	3

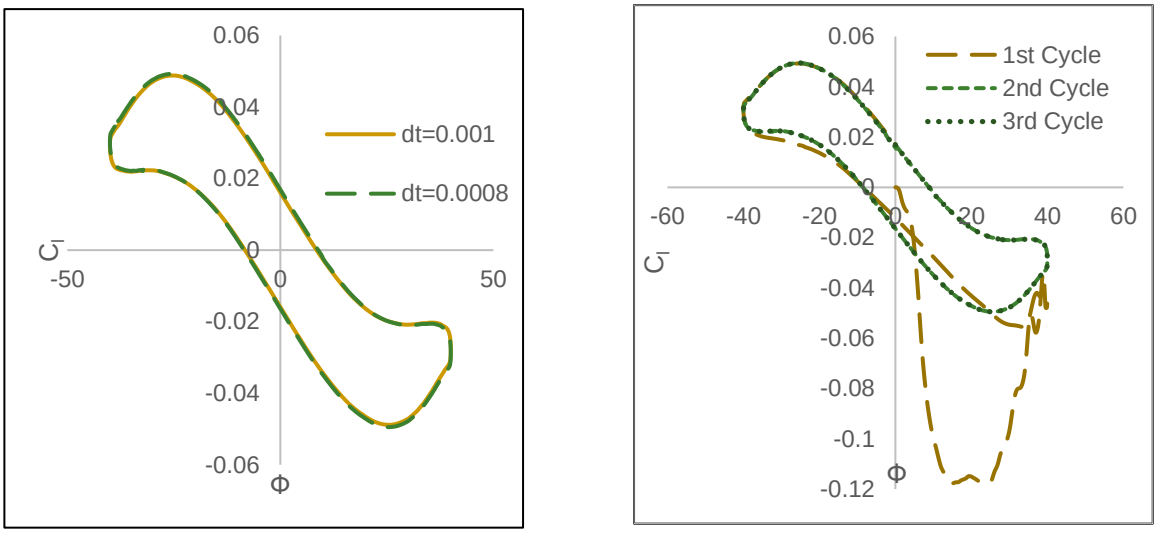

Figure 4–Time step independence and convergence criteria

3. Results and Discussion

The static stability loops are for angles of attack 0°-25°, as shown in Figure 5. The slope of the static stability loops represents the static stability derivative in roll $C_{;L\phi}$. It is noticed that for all angles of attack from 0°-25°, the value of static stability derivative is negative. The negative slope of the static stability loops in Figure 5 shows that the rectangular wing of aspect ratio two has the inherent initial tendency to return to its original equilibrium position of 0° roll angle after a roll angle of 40° amplitude has perturbed it. Hence the wing is statically stable for angles of attack $0° - 25°$.

The dynamic stability loops for angles of attack 0°-25° are shown in Figure 6, in which the rolling moment coefficient is plotted against the non-dimensional rolling rate. The slope of the dynamic stability loops represents the dynamic roll damping parameter C_{Lp}. It is noticed that for angles of attack from 0°-15°, the values of the roll damping parameter are negative. The slope of the loop becomes positive at 20° angle of attack.

The positive slope of the roll damping parameter at the 20° angle of attack indicates that the rectangular wing of aspect ratio two will keep oscillating around its statically equilibrium position of the roll angle of 0° . Hence it gets dynamically unstable at 20° angle of attack. It indicates the onset of the wing rock phenomenon.

A three-degree polynomial curve fitting was done on the numerical results of the roll damping parameter as the best fit to evaluate its variation to the angle of attack, as shown in Figure 7. The curve fitting revealed that the rectangular wing of aspect ratio two becomes dynamically unstable somewhere between 15° and 20° angle of attack. The rectangular wing of aspect ratio two stalled at 20° angle of attack. Hence, the wing rock phenomenon starts to occur in the vicinity of the stall.

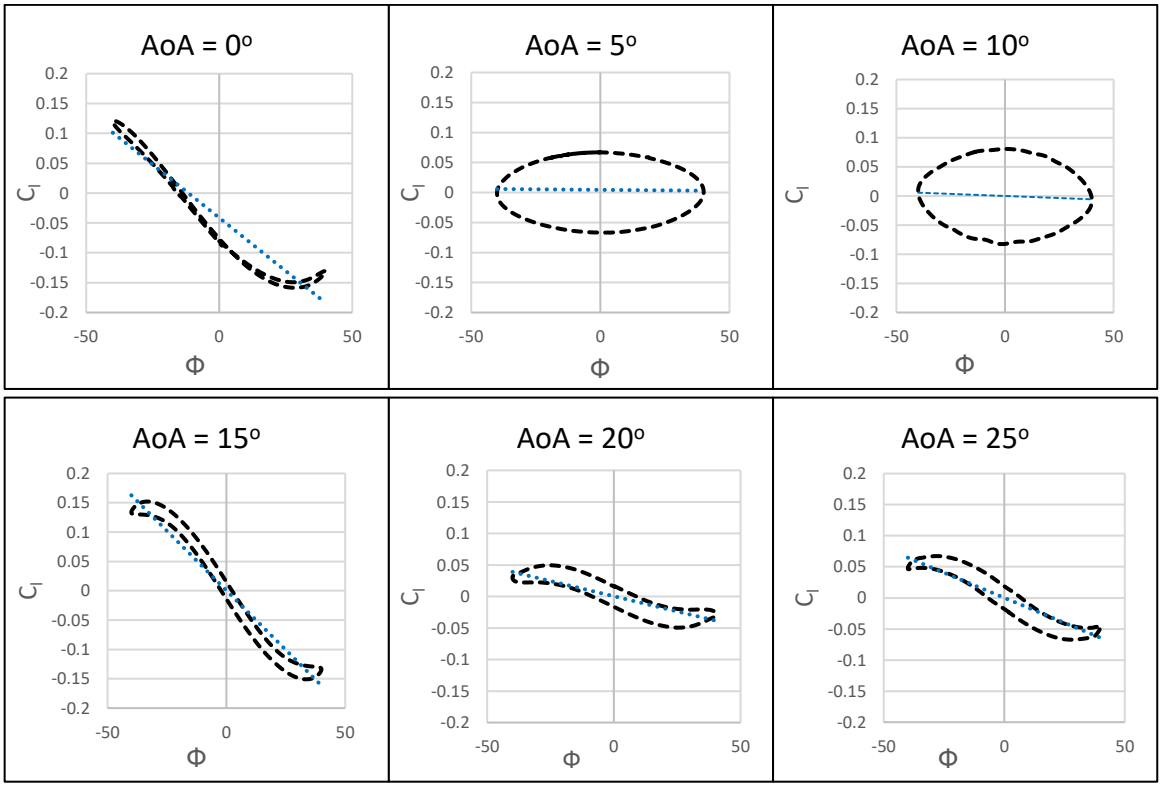

Figure 5 – Rolling moment coefficient with change in roll angle

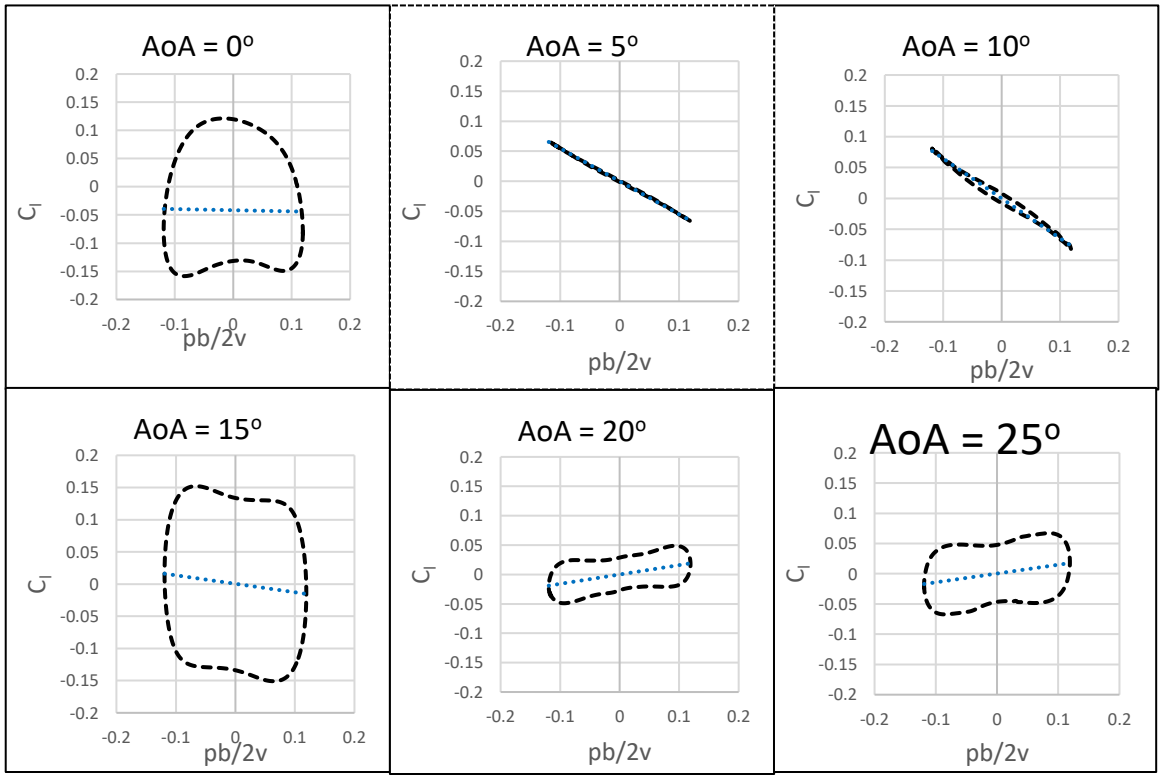

Figure 6 – Rolling moment coefficient with change in non-dimensional roll rate

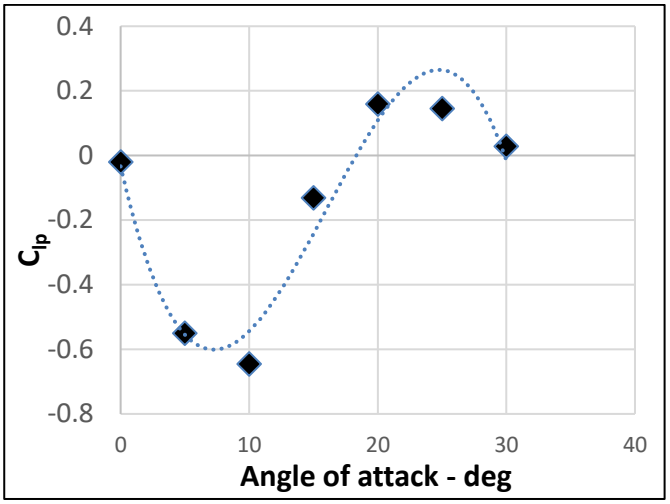

Figure 7 – Roll moment damping coefficient with the change in angle of attack

During forced roll oscillations, it was noticed that the side of the wing, which was moving in an upward direction, had a powerful tip vortex attached to it compared to the lower side, which had a small weak tip vortex, as shown in Figure 8. It was also observed that as the side of the wing, which was moving in an upward direction, reached its maximum amplitude and it was about to rotate in the opposite direction, the tip vortex on the lower side of the wing also started to grow in size as shown in Figure 8. Similar observations were made when the left side of the wing was moving in an upward direction.

On extraction of flow attachment lines, it was revealed that these flow attachment lines are present on that side of the wing, which had a strong tip vortex. A similar observation was made when the left side of the wing moved upward and had a strong tip vortex. Strong tip vortices present on the tips of the wing are low pressure regions. The surrounding flow is drawn over these low-pressure regions resulting in an inboard attachment of flow, giving rise to the nonlinear vortex lift.

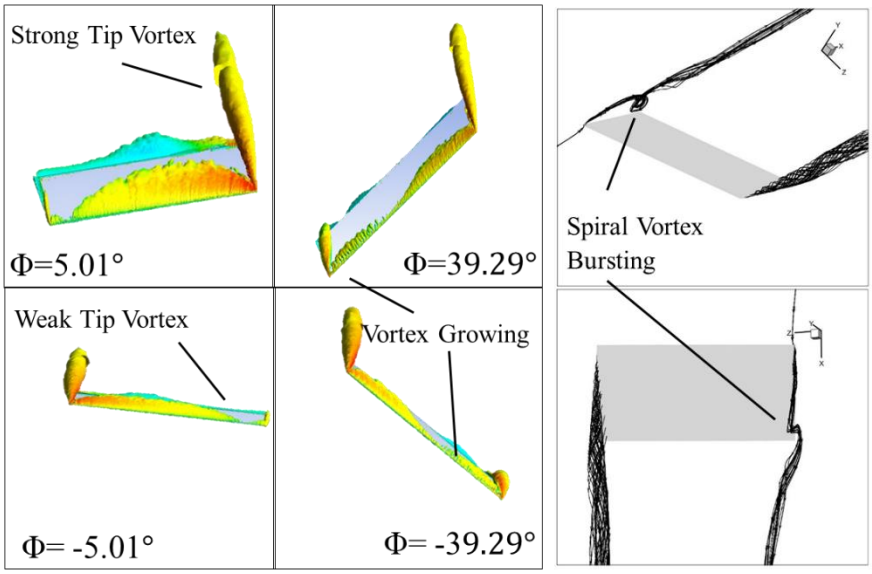

Figure 8 – Vortices generated during roll oscillations

To link the numerical finding on roll damping parameter with flow physics of the vortical structures present on the wing, an in-depth post-processing study was done for the dynamically stable case of 10° and the dynamically unstable case of 20°. Post-processing revealed that for the dynamically stable case of 10 ° angle of attack, the tip vortices remain intact with the tips of the wing during the whole cycle of oscillation, as shown in Figure 9.

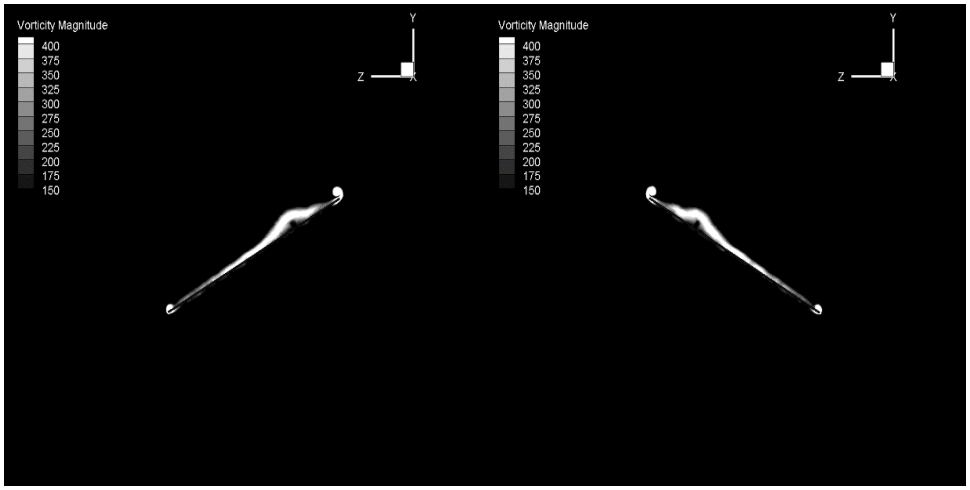

Figure 9 –Tip vortices for dynamically stable case at angle of attack of 10 deg

For the dynamically unstable case of 20° angle of attack, the tip vortices started to burst into the leading edge separated vortex. The wing reaches its maximum amplitude of 40° roll angle, as shown in Figure 10. The interaction of tip vortices with leading-edge separated vortex is postulated to be the main reason for the sustenance of these roll oscillations.

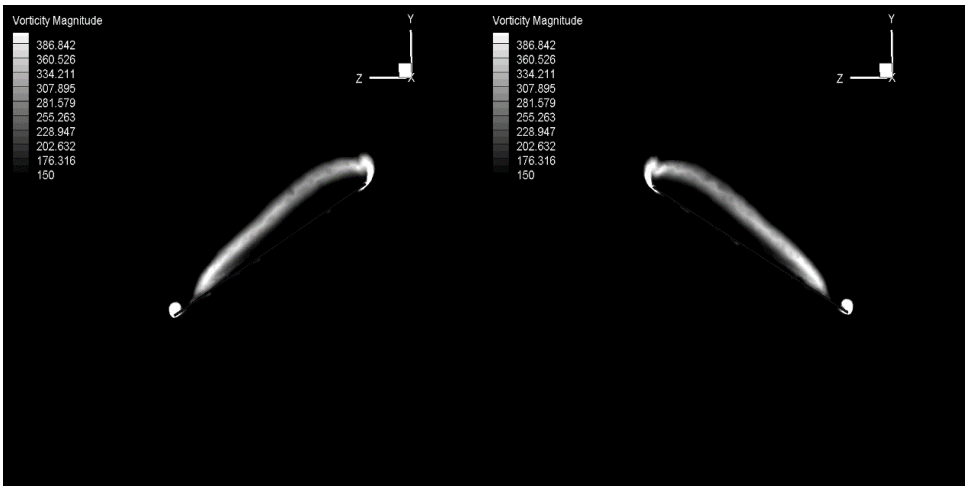

Figure 10 –Tip vortices for dynamically unstable case at angle of attack of 20 deg

4. Conclusion

In this research, forced roll oscillations were applied on the rectangular wing of aspect ratio 2. The resulting qualitative characteristics of the flow on the application of forced roll oscillations resemble with the flow behavior during free-to-roll oscillations. It is concluded that the rectangular wing of aspect ratio 2 is statically stable in roll for angles of attack 0° -30°. Side tip vortices remain intact with the sides of the wing over the whole cycle of the oscillation to ensure dynamic stability of the wing. The onset of dynamic instability occurs at an angle of attack between 15° and 20°. The dynamic instability occurs due to the vortex bursting or vortex breakdown phenomenon and its interaction with the leading-edge main vortex. The difference in vortex core positions of the left and right-side tip vortex contribute to the dynamic instability of the wing.

5. Contact Author Email Address

adnan@rcms.nust.edu.pk

6. Copyright Statement

References

[1] ARENA, JR, A., and R. Nelson. The effect of asymmetric vortex wake characteristics on a slender delta wing undergoing wing rock motion. *16th AIAA Atmospheric Flight Mechanics Conference*, Boston, U.S.A. AIAA 89-3348-CP, 1989.

[2] Go T. H. and Ramnath R. V. An Analytical Approach to the Aircraft Wing Rock Dynamics. *AIAA Atmospheric Flight Mechanics Conference and Exhibit*, Montreal, Canada. AIAA 2001-4426, 2001

[3] Ross A. J. and Nguyen L. T. *Some observations regarding wing-rock oscillations at high angles of attack*. RAE, 1988.

[4] Ericsson L. E. The Fluid Mechanics of Slender Wing Rock. *Journal of Aircraft*, Vol. 21, No. 5, pp 22-328, 1984.

[5] Ericsson, L. E. Flow Phenomena Causing Wing and Body Rock. *2nd AIAA Applied Aerodynamics Conference*, Seattle, WA, USA. 1984.

[6] Gresham N. T., Wang Z. and Gursul I. Vortex Dynamics of Free-to-Roll Slender and Nonslender Delta Wings. *Journal of Aircraft*, Vol. 47, No. 1, pp 292-302, 2010.

[7] Jun Y. W. and Nelson R. C. Leading edge vortex dynamics on a delta wing undergoing a wing rock motion. *25th AIAA Aerospace Sciences Meeting*, Reno, NV, U.S.A. 1987.

[8] Arena A. S. and Nelson R. C. Experimental investigations on limit cycle wing rock of slender wings. *Journal of Aircraft*, Vol. 31, No. 5, pp 1148-1155, 1994.

[9] Ross A. J. Investigation of nonlinear motion experienced on a slender-wing research aircraft. *Journal of Aircraft*, Vol. 9, No. 9, 1972.

[10] Nguyen L., Yip L., and Chambers J. Self-induced wing rock of slender delta wings. *7th AIAA Atmospheric Flight Mechanics Conference*, Albuquerque, NM, U.S.A. 1981.

[11] Gabriel E. T. and Mueller T. J. Low Aspect Ratio Wing Aerodynamics at Low Reynolds Numbers. *AIAA Journal*, Vol. 42, No. 5, pp 865-873, 2004.

[12] Maqsood, A. and Go, T.H. Aerodynamic characteristics of a flexible membrane micro air vehicle. *Aircraft Engineering and Aerospace Technology*, Vol. 87, No. 1, pp 30-37, 2015.

[13] Mir, I., Maqsood, A., Eisa, S. A., Taha, H. and Akhtar, S. Optimal morphing – augmented dynamic soaring maneuvers for unmanned air vehicle capable of span and sweep morphologies. *Aerospace Science and Technology*, Vol. 79, pp 17-36, 2018.

[14] Umer, H. M., Maqsood, A., Riaz, R. and Salamat, S. Stability Characteristics of Wing Span and Sweep Morphing for Small Unmanned Air Vehicle: A Mathematical Analysis. *Mathematical Problems in Engineering*, Vol. 2020, pp 1-15, 2018.

[15] Maqsood, A. and Go, T.H. Parametric Studies and Performance Analysis of a Biplane Micro Air Vehicle. *International Journal of Aeronautical and Space Sciences*, Vol. 14, No. 3, pp 229-236, 2013.

[16] Maqsood, A. and Go, T.H. Optimization of transition maneuvers through aerodynamic vectoring. *Aerospace Science and Technology*, Vol. 23, No. 1, pp 363-371, 2012.

[17] Cosyn P. and Vierendeels J. Numerical Investigation of Low-Aspect-Ratio Wings at Low Reynolds Numbers. *Journal of Aircraft*, Vol. 43, No. 3, pp 713-722, 2006.

[18] Go T. H. and Maqsood A. Effect of aspect ratio on wing rock at low Reynolds number. *Aerospace Science and Technology*, Vol. 42, pp 267-273, 2015.